Optics Communications 451 (2019) 290–295

Contents lists available at ScienceDirect

Optics Communications

journal homepage: www.elsevier.com/locate/optcom

Analysis of a flat-top optical ring resonator

Menghao Huang, Simin Li *, Zhizhi Yang, Shilong Pan

Key Laboratory of Radar Imaging and Microwave Photonics, Ministry of Education, Nanjing University of Aeronautics and Astronautics, Nanjing 210016, China

ARTICLE INFO

Keywords:
Microring resonator
True time delay
Integrated optics

ABSTRACT

In this paper, a theoretical analysis of a flat-top microring resonator (FTMRR) is undertaken. The intensity and group delay responses of the FTMRR are derived from a transfer matrix formalism, which shows that flat-top resonance is possible in this single-ring cavity by stimulating and manipulating slow light in the counterclockwise (CCW) mode and fast light in the clockwise (CW) mode. The analytical solutions required for achieving the flat-top responses are obtained by assuming that the slope around the resonant wavelength equals zero. In addition, an improvement in the bandwidth of the FTMRR (in comparison with the MRR), the tunable and reconfigurable optical responses for filtering/switching, and the small variation in intensity during the tuning of the flat-top group delay observed in the previous experiments are all proved through theoretical analysis.

1. Introduction

Optical microring resonators (MRRs) have been regarded as the basic building blocks in photonic integrated circuits (PICs) [1], which can realize optical filters [2], time delay lines [3], wavelength division multiplexers [4], optical sensors [5], modulators [6], lasers [7], optical switches [8], optical diodes [9], and photonic interconnects [10] with very small footprints. In general, the intensity and the group delay responses of an MRR around the resonant wavelengths are Lorentzian-shaped, resulting in a small bandwidth [11], which is not suitable for broadband microwave photonics applications. Although cascading several MRRs can synthesize a large bandwidth [12,13], the devices are not easy to create and the insertion loss is a huge challenge for microwave photonics applications, which may cause undesired effects when the group delay needs to be tuned [14]. In addition, sophisticated adjustments are required to ensure that all the MRRs are precisely aligned to the designated parameters. In [15,16], it has been observed that backscattering in a silicon MRR may cause mode splitting due to the combined effects of the counterclockwise (CCW) and clockwise (CW) propagating light in the cavity. However, this backscattering is normally random and uncontrollable, which is usually treated as a problem. Recently, we have experimentally demonstrated a new optical microring resonator that stimulates flat-top resonance by manipulating the fast and slow light effects in the ring cavity [17], and the measured results obtained from an optical vector analyzer [18,19] match numerical simulations well. In the flat-top optical microring resonator (FTMRR), a reflector is incorporated in the drop port of a conventional add-drop MRR to form both the CCW mode (slow light) and the CW mode (fast light), as shown in Fig. 1(a). The strengths of the slow and fast light are controlled by the coupling coefficients of the upper and lower couplers of the FTMRR. The FTMRR has three operating states in terms of both the intensity and group delay responses: Lorentzian, mode splitting, and flat-top, all of which indicate that it can be used in many microwave photonics applications that are either difficult or impossible for a conventional single MRR such as a tunable wideband optical true time delay line, a shape-reconfigurable optical filter, a high-extinction-ratio optical switch, and so on.

In this paper, we perform a comprehensive study of the FTMRR. The intensity and group delay responses of the FTMRR are derived based on the transfer matrix formalism [1]. Then, the analytical solutions for achieving the flat-top responses are obtained by assuming that the slope of the intensity or the group delay response around the resonant wavelength equals zero. By bringing the analytical solutions into the intensity and group delay responses, the experimental observation of the flat-top intensity and group delay responses are explained, which intuitively illustrate the enhanced performance of the FTMRR through comparisons with the conventional MRR since they act as basic building blocks in a single cavity.

2. Theoretical analysis

Fig. 1(a) shows the configuration of the proposed FTMRR, which consists of a single MRR and a reflector (loop mirror) incorporated into the drop port of the MRR. The incident light from Port 1 is coupled with the ring cavity and then propagates along the CCW direction (CCW mode). Then, the output light is reflected back to the ring cavity by the reflector and propagates along the CW direction (CW mode).

* Corresponding author.
E-mail address: lisimin@nuaa.edu.cn (S. Li).

https://doi.org/10.1016/j.optcom.2019.06.038
Received 1 March 2019; Received in revised form 8 May 2019; Accepted 14 June 2019
Available online 26 June 2019

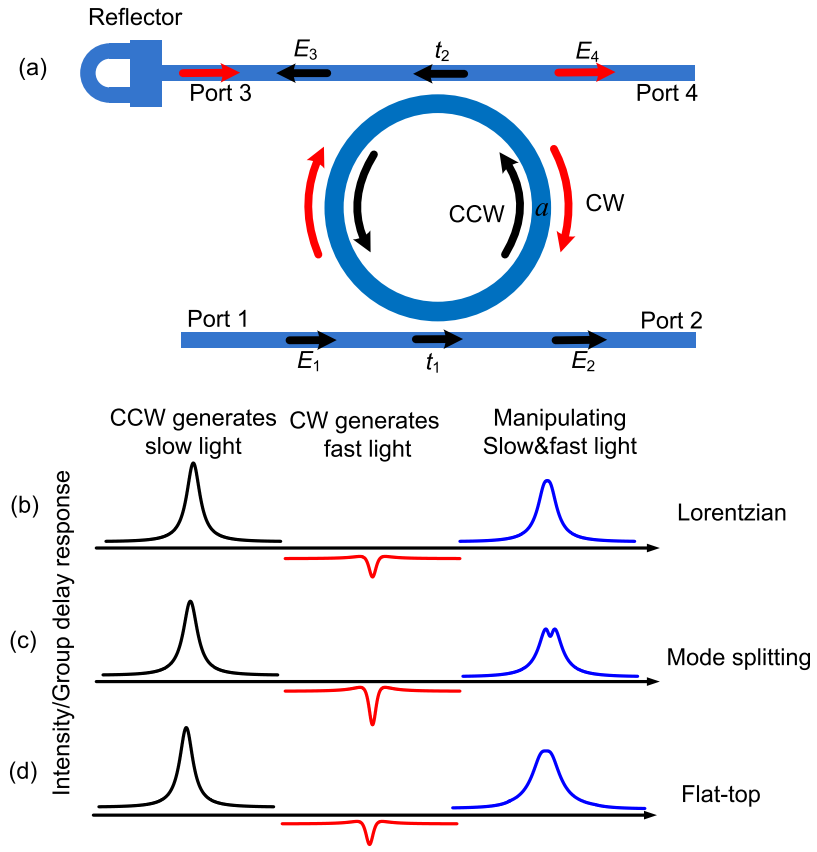

Fig. 1. The FTMRR and the responses for the three states. (a) A schematic diagram of the FTMRR, and the intensity/group delay responses for the (b) Lorentzian, (c) mode splitting, and (d) flat-top states.

For the CCW mode, the ratio of the electrical field at the through port (Port 2) E_2 and the incident field E_1 can be expressed as [1]

$$\frac{E_2}{E_1} = \frac{t_1 - at_2 e^{i\phi}}{1 - at_1 t_2 e^{i\phi}} \tag{1}$$

where $\phi = \beta L$ is the single-pass phase shift, $L = 2\pi r$, r is the radius of the microring, β is the propagation constant of the circulating mode, a is the single-pass amplitude transmission coefficient, t_1, t_2 are the self-coupling coefficients, and k_1, k_2 are the cross-coupling coefficients. If there are no losses in the coupling sections, we obtain

$$t_n^2 + k_n^2 = 1 \quad (n = 1, 2) \tag{2}$$

Then, the group delay for the light at Port 2 can be written as

$$\tau_2 = \left(\frac{a^2 t_2^2 - at_1 t_2 \cos\phi}{a^2 t_2^2 + t_1^2 - 2at_1 t_2 \cos\phi} + \frac{at_1 t_2 \cos\phi - a^2 t_1^2 t_2^2}{1 + a^2 t_1^2 t_2^2 - 2at_1 t_2 \cos\phi} \right) \frac{n_g L}{c} \tag{3}$$

where n_g is the group index, and c is the speed of light in a vacuum.

The ratio of E_3 at Port 3 and E_1 can be expressed as

$$\frac{E_3}{E_1} = \frac{-\sqrt{a} k_1 k_2 e^{\frac{i\phi}{2}}}{1 - at_1 t_2 e^{i\phi}} \tag{4}$$

and the group delay for the light at Port 3 is given by

$$\tau_3 = \left(\frac{1}{2} + \frac{at_1 t_2 \cos\phi - a^2 t_1^2 t_2^2}{1 + a^2 t_1^2 t_2^2 - 2at_1 t_2 \cos\phi} \right) \frac{n_g L}{c} \tag{5}$$

Around the resonant wavelength, i.e. $\cos\phi \approx 1$, (5) can be rewritten as

$$\tau_3 = \frac{1 + at_1 t_2}{2\left(1 - at_1 t_2\right)} \frac{n_g L}{c} \tag{6}$$

It can be seen that (6) is always positive, so the slow-light effect occurs when the light travels from Port 1 to Port 3.

For the CW mode, similar to (1), the ratio of the electrical field at Port 4 E_4 and the incident field E_3 can be expressed as

$$\frac{E_4}{E_3} = \frac{\eta\left(t_2 - at_1 e^{i\phi}\right)}{1 - at_1 t_2 e^{i\phi}} \tag{7}$$

where η represents the reflectivity of the loop mirror. The group delay for the light from Port 3 to Port 4 is given by

$$\tau_4 = \left(\frac{a^2 t_1^2 - at_1 t_2 \cos\phi}{a^2 t_1^2 + t_2^2 - 2at_1 t_2 \cos\phi} + \frac{at_1 t_2 \cos\phi - a^2 t_1^2 t_2^2}{1 + a^2 t_1^2 t_2^2 - 2at_1 t_2 \cos\phi} \right) \frac{n_g L}{c} \tag{8}$$

Around the resonant wavelength, i.e. $\cos\phi \approx 1$, (8) can be simplified as

$$\tau_4 = \frac{at_1\left(1 - t_2^2\right)}{\left(at_1 - t_2\right)\left(1 - at_1 t_2\right)} \frac{n_g L}{c} \tag{9}$$

From (9), if $t_2 \leq at_1$ (the over coupling and critical coupling states), τ_4 is positive, so the slow-light effect occurs. On the other hand, if $t_2 > at_1$ (the under coupling state), the fast-light effect will be stimulated. In this paper, we only take the fast light condition $t_2 > at_1$ into consideration.

From (4) and (7), we can easily get the ratio of E_4 and E_1,

$$\frac{E_4}{E_1} = \frac{-\eta\sqrt{a} k_1 k_2 e^{\frac{i\phi}{2}} \left(t_2 - at_1 e^{i\phi}\right)}{\left(1 - at_1 t_2 e^{i\phi}\right)^2} \tag{10}$$

The intensity response T can therefore be expressed as

$$T = \left|\frac{E_4}{E_1}\right|^2 = \frac{\eta^2 a (1 - t_1^2)(1 - t_2^2)\left(a^2 t_1^2 + t_2^2 - 2at_1 t_2 \cos\phi\right)}{\left[1 + \left(at_1 t_2\right)^2 - 2at_1 t_2 \cos\phi\right]^2} \tag{11}$$

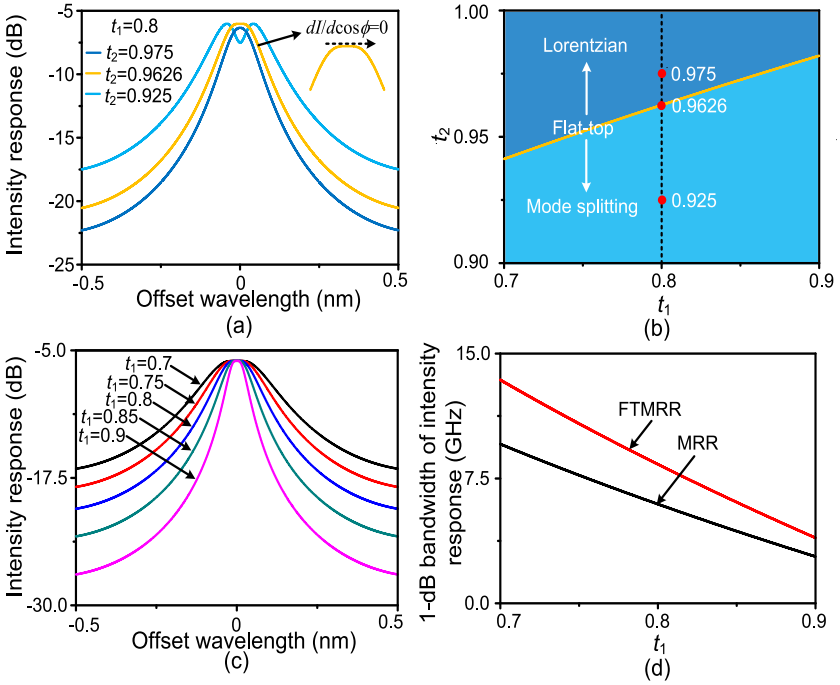

Fig. 2. Investigation of the intensity response of the FTMRR. (a) The intensity response when t_1 is fixed at 0.8 and t_2 is set to be three typical values (0.975, 0.9626, and 0.925). (b) The relationship of t_1 and t_2 for Lorentzian, flat-top, and mode splitting intensity responses. (c) The flat-top intensity responses when t_1 and t_2 are adjusted. (d) The 1-dB bandwidth of intensity response for the MRR and FTMRR as a function of t_1.

In addition, the total group delay for the light traveling from Port 1 to Port 4 is a sum of (5) and (8), i.e.

$$\tau_{\text{total}} = \left(\frac{1}{2} + \frac{a^2 t_1^2 - a t_1 t_2 \cos\phi}{a^2 t_1^2 + t_2^2 - 2 a t_1 t_2 \cos\phi} + \frac{2(a t_1 t_2 \cos\phi - a^2 t_1^2 t_2^2)}{1 + a^2 t_1^2 t_2^2 - 2 a t_1 t_2 \cos\phi} \right) \frac{n_g L}{c} \tag{12}$$

From (11) and (12) we can see that changing the reflectivity of the reflector only adds an additional loss to the FTMRR, while the intensity response and the group delay response remain the same shape.

Around the resonant wavelength, i.e. $\cos\phi \approx 1$, (11) and (12) can be simplified to

$$T = \frac{\eta^2 a (1 - t_1^2)(1 - t_2^2)(a t_1 - t_2)^2}{(1 - a t_1 t_2)^4} \tag{13}$$

$$\tau = \left(\frac{1}{2} + \frac{a t_1}{a t_1 - t_2} + \frac{2 a t_1 t_2}{1 - a t_1 t_2} \right) \frac{n_g L}{c} \tag{14}$$

There are two extreme cases. One case is that the fast light effect is small enough to be ignored, so the total response has a Lorentzian shape, corresponding to the case illustrated in Fig. 1(b). In this case, the FTMRR functions as a conventional MRR. The other case is that the fast light effect plays a dominant role, so there is mode splitting in the total response, as shown in Fig. 1(c). Through the proper manipulation of the fast and slow light effects, a flat-top response can be obtained, as shown in Fig. 1(d).

To achieve the flat-top intensity response, the slope of (11) around the resonant wavelength should equal zero. The first derivative of the intensity response can be expressed as

$$\frac{dT}{d\cos\phi} = \frac{-2 a^2 t_1 t_2 (1 - t_1^2)(1 - t_2^2)\left[1 + (a t_1 t_2)^2 - 2 a^2 t_1^2 - 2 t_2^2 + 2 a t_1 t_2 \cos\phi\right]}{\left[1 + (a t_1 t_2)^2 - 2 a t_1 t_2 \cos\phi\right]^3} \tag{15}$$

Table 1
All states of the FTMRR.

t_1 and t_2 relationship	Intensity response	Group delay response
$t_2 > \frac{1+\sqrt[3]{2}at_1}{\sqrt[3]{2}+at_1}$	Lorentzian	Lorentzian
$t_2 = \frac{1+\sqrt[3]{2}at_1}{\sqrt[3]{2}+at_1}$	Lorentzian	Flat-top
$\frac{1+\sqrt{2}at_1}{\sqrt{2}+at_1} < t_2 < \frac{1+\sqrt[3]{2}at_1}{\sqrt[3]{2}+at_1}$	Lorentzian	Mode splitting
$t_2 = \frac{1+\sqrt{2}at_1}{\sqrt{2}+at_1}$	Flat-top	Mode splitting
$at_1 < t_2 < \frac{1+\sqrt{2}at_1}{\sqrt{2}+at_1}$	Mode splitting	Mode splitting
$t_2 \le at_1$	Mode splitting	Lorentzian

Let $dT/d\cos\phi = 0$ (around the resonant wavelength $\cos\phi \approx 1$) and we get the analytical solution for the flat-top intensity response

$$t_2 = (1 + \sqrt{2} a t_1)/(\sqrt{2} + a t_1) \tag{16}$$

Similarly, the first derivative of the group delay can be expressed as

$$\frac{d\tau}{d\cos\phi} = \left(\frac{a^3 t_1^3 t_2 - a t_1 t_2^3}{(a^2 t_1^2 + t_2^2 - 2 a t_1 t_2 \cos\phi)^2} + \frac{2(a t_1 t_2 - a^3 t_1^3 t_2^3)}{(1 + a^2 t_1^2 t_2^2 - 2 a t_1 t_2 \cos\phi)^2} \right) \frac{n_g L}{c} \tag{17}$$

The flat-top group delay can be achieved when $d\tau/d\cos\phi = 0$ (around the resonant wavelength $\cos\phi \approx 1$), leading to

$$\frac{a t_1 + t_2}{1 + a t_1 t_2} = \frac{-2(a t_1 - t_2)^3}{(1 - a t_1 t_2)^3} \tag{18}$$

To achieve weak, fast light in the CW, t_2 should be close to 1, so we get

$$\frac{a t_1 + t_2}{1 + a t_1 t_2} \approx 1 \tag{19}$$

Bringing (19) into (18), we can achieve the analytical solution for the flat-top group delay response

$$t_2 = (1 + \sqrt[3]{2} a t_1)/(\sqrt[3]{2} + a t_1) \tag{20}$$

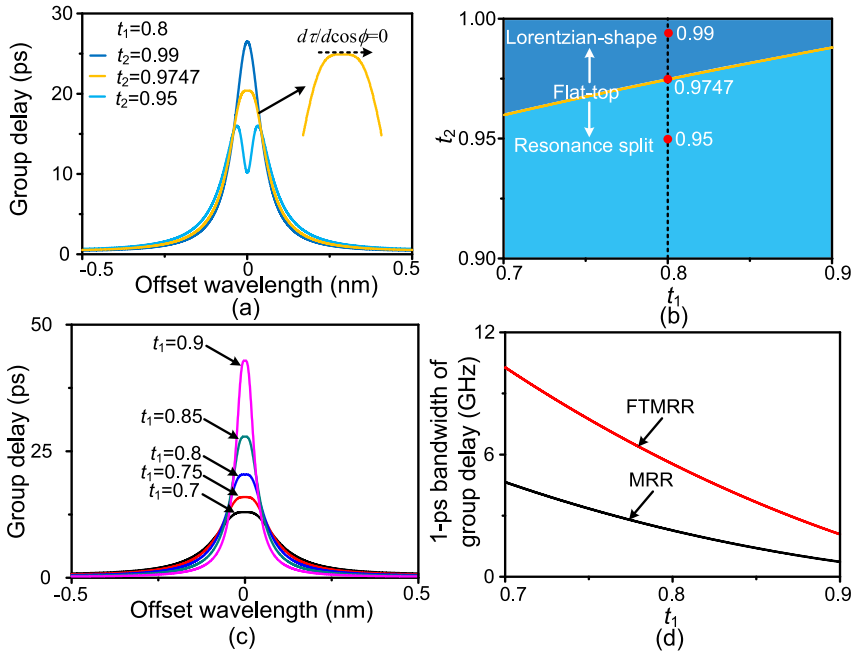

Fig. 3. Investigation of the group delay response for the FTMRR. (a) The group delay response of the FTMRR with t_1 fixed at 0.8 and t_2 changed from 0.99 (Lorentzian), 0.9847 (flat-top), to 0.95 (mode splitting). (b) The relationship of t_1 and t_2 for Lorentzian, flat-top, and mode splitting group delay responses. (c) The flat-top group delay responses when t_1 and t_2 are adjusted. (d) The 1-ps bandwidth of the group delay for both FTMRR and MRR as a function of t_1.

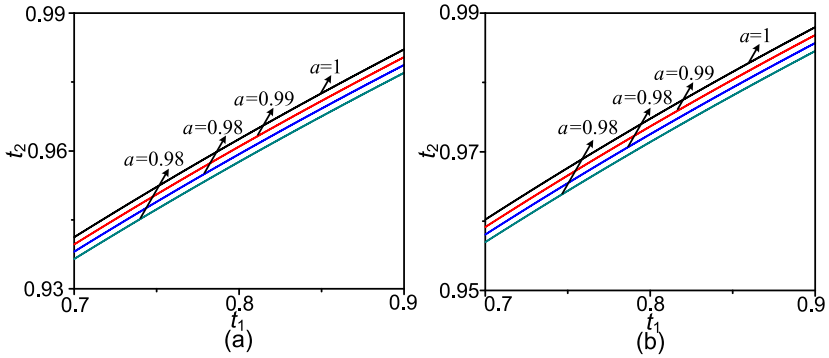

Fig. 4. The flat-top conditions with different losses. (a) The flat-top intensity response conditions with different a. (b) The flat-top group delay response conditions with different a.

Table 1 shows all the operational states of the FTMRR and the corresponding intensity and group delay responses. The results indicate that it is not possible to realize the flat-top intensity and group delay response at the same time. Furthermore, the flat-top group delay response always has a Lorentzian intensity response, which is a passband with a lower insertion loss compared to the MRR time delay line operating in the all-pass mode [2].

3. Simulation and results

In this section, the performance of the FTMRR is simulated using parameters of $r = 100$ μm, $n_g = 3.24$, and a resonant wavelength $\lambda = 1549.17857$ nm. The waveguide is assumed to be lossless; i.e. $a = 1$.

Fig. 2(a) shows the simulated intensity response when t_1 is fixed at 0.8 and t_2 is set to be three typical values for different operating states of the FTMRR. According to (7), the notch response from Port 3 to Port 4 becomes deeper if t_2 is approaching at_1, so the response from Port 1 to Port 4 changes from Lorentzian ($t_2 = 0.975$) to flat-top ($t_2 = 0.9626$) to mode splitting state ($t_2 = 0.925$) successively. The notch of the mode splitting state could be very deep as t_2 is near at_1, so the intensity response can be changed easily from bandpass to notch, as seen in Fig. 2(b) in [17], indicating that the FTMRR can be used as a shape-reconfigurable optical filter or a high-extinction-ratio optical switch. Fig. 2(b) shows that there is a one-to-one correspondence between t_1 and t_2 in achieving the flat-top intensity response. The Lorentzian and mode splitting conditions are also depicted. Fig. 2(c) shows the intensity response for different t_1 and t_2 satisfying the flat-top conditions, while the bandwidth is increased with a decrease in t_1, which agrees well with the experiment's results in [17]. The comparison of the 1-dB bandwidth between FTMRR and MRR is shown in Fig. 2(d). With t_1 tuned from 0.7 to 0.9, the 1-dB bandwidth for the FTMRR can be tuned from 3.94 to 13.43 GHz, while the MRR can be tuned from 2.8–9.57 GHz. It should be mentioned that in order to realize a wide range and accurate tuning of the coupling coefficients, an MZI structure is preferred, as in [17].

Fig. 3(a) shows the simulated group delay response when t_1 is fixed at 0.8 and t_2 is set to be three typical values. With a decreasing t_2, the fast-light effect gradually increases. Calculated from (20), there is also a one-to-one correspondence between t_1 and t_2 in order to obtain the flat-top group-delay response. Fig. 3(b) reveals this relationship, which also illustrates the Lorentzian and mode splitting conditions. Fig. 3(c) shows that the flat-top group delay can be tuned by adjusting t_1 and t_2. The group delay increases continuously with an increase in t_1 while

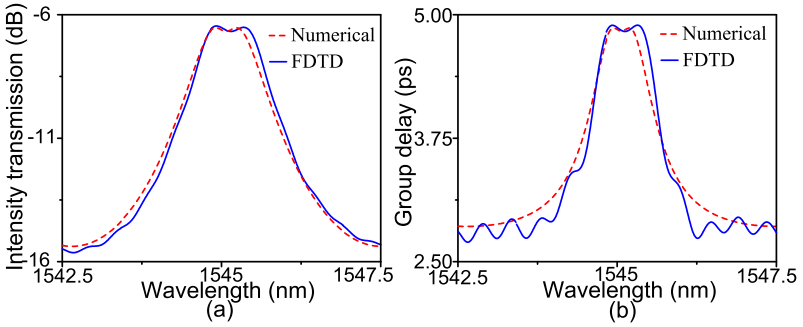

Fig. 5. Comparison of the numerical and FDTD simulation results. (a) Numerical and FDTD simulation results for the flat-top intensity response. (b) Numerical and FDTD simulation results for the flat-top group delay responses.

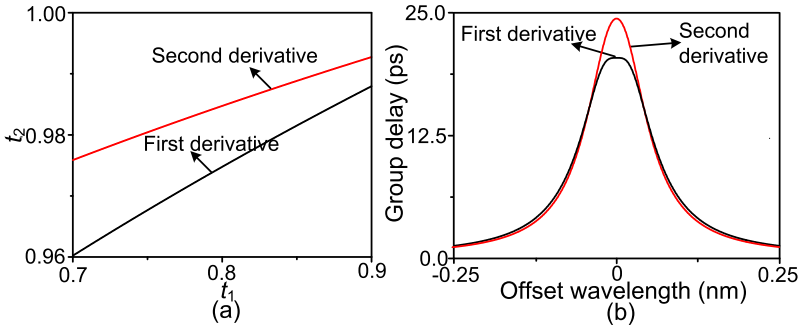

Fig. 6. The comparison between the two flat-top group delay criteria. (a) The second and the first derivative. (b) An example of the group response with the two criteria.

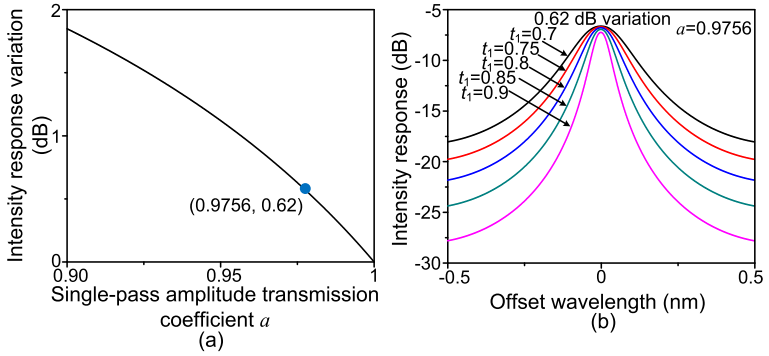

Fig. 7. Investigation of the intensity response variation during the flat-top group delay tuning. (a) The intensity response variation as a function of a when t_1 has a tuning range between 0.7 and 0.9. (b) The intensity response for the case $a = 0.9756$.

the bandwidth decreases. These results agree very well with Fig. 3(a) in [17]. Fig. 3(d) shows the 1-ps group delay bandwidth for the FTMRR with t_1 tuned from 0.7 to 0.9. The value for the FTMRR can be tuned from 2.09 to 10.28 GHz, while the MRR can only be from 0.73 to 4.65 GHz.

The waveguide is assumed to be lossless in order to simplify the simulation. However, there is loss in the ring resonator in practice. Fig. 4(a) and (b) show the flat-top intensity and group delay conditions with different a according to (16) and (20), from which we can ascertain that the flat-top states can still be reached with a loss in the ring. Meanwhile, t_2 correlates positively with a if t_1 is kept unchanged.

The Finite-Difference Time-Domain (FDTD) method is also investigated in order to verify the flat-top states, and the simulation parameters are: $r = 23$ μm, $n_g = 3.24$, $a = 0.5$ dB/cm. Fig. 5(a) and (b) are comparisons between the FDTD and the numerical simulation results with the same parameters for both flat-top intensity and group delay responses, showing that the numerical simulation results match the FDTD simulation results well.

It should be mentioned that in [17], we used the second derivative of the group-delay response to obtain the flat-top condition and found that there is a slight deviation from the ideal values of t_1 and t_2. In this work, a corrected criterion for the flat-top group delay is provided based on the first derivative. A comparison between the two flat-top group delay criteria is given in Fig. 6(a), which shows that the flat-top condition obtained by the second derivative is different from those obtained by the first derivative. Fig. 6(b) shows the group delay responses under the two conditions. It can be seen that the flat-top condition obtained by the first derivative is more accurate.

From (13) we can see that for a given t_1 and t_2, the insertion loss is a function of a at the resonant wavelength. Within a certain tuning range of t_1 and t_2 (here we set t_1 to change from 0.7 to 0.9, and t_2 to satisfy the flat-top group delay condition), the intensity loss variation is calculated as a function of a. As shown in Fig. 7(a), during the flat-top group delay tuning, the insertion loss variation decreases from 1.85 to 0 dB with a changing from 0.9 to 1, which indicates that if the loss in the ring cavity is very small, the insertion loss variations could even be ignored. For a silicon nitride waveguide in [17], the loss for the waveguide is less than 0.5 dB/cm and the ring cavity is 4293.9 m long, corresponding to $a \geq 0.9756$. As depicted in Fig. 7(a), the intensity loss variation is 0.62

dB, which corresponds with the measured result in [17] (less than 0.8 dB). Fig. 7(b) shows the intensity response for the case of $a = 0.9756$, which gives the 0.62 dB intensity loss variation.

4. Conclusions

In conclusion, the analytical model of the FTMRR is built from the transfer matrix formalism of a conventional MRR. The relationship between t_1 and t_2 in order to achieve the flat-top intensity and the group delay is obtained. Typical operational states of the FTMRR are simulated. The advantages of the FTMRR observed in the experiment in [17] are theoretically explained, including the bandwidth improvement of the FTMRR in comparison with the MRR, tunable and reconfigurable optical responses for filtering/switching, and the small intensity variation during the tuning of the flat-top group delay. This analysis could be a guidance in optimizing the structure of the FTMRR for microwave photonic applications.

Acknowledgment

This work was supported by "the Fundamental Research Funds for the Central Universities", China (NS2016045).

References

[1] W. Bogaerts, P.D. Heyn, T.V. Vaerenbergh, K.D. Vos, S.K. Selvaraja, T. Claes, P. Dumon, P. Bienstman, D.V. Thourhout, R. Baets, Silicon.microring. resonators, Las. Photon. Rev, Silicon microring resonators, Laser Photon. Rev. 6 (1) (2012) 47–73.

[2] L. Zhang, H. Zhao, H. Wang, S. Shao, W. Tian, J. Ding, X. Fu, L. Yang, CaScading second-order microring resonators for a box-like filter response, J. Lightw. Technol. 35 (24) (2017) 5347–5360.

[3] J. Cardenas, M. Foster, N. Sherwood-Droz, C. Poitras, H. Lira, B. Zhang, A. Gaeta, J. Khurgin, P. Morton, M. Lipson, Wide-bandwidth continuously tunable optical delay line using silicon microring resonators, Opt. Express 18 (25) (2010) 26525–26534.

[4] S. Wang, X. Feng, S. Gao, Y. Shi, T. Dai, H. Yu, H. Tsang, D. Dai, On-chip reconfigurable optical add-drop multiplexer for hybrid wavelength/mode-division-multiplexing systems, Opt. Lett. 42 (14) (2017) 2802–2805.

[5] H.H. Zhu, Y.H. Yue, Y.J. Wang, M. Zhang, L.Y. Shao, J.J. He, M.Y. Li, High-sensitivity optical sensors based on cascaded reflective MZIs and microring resonators, Opt. Express 25 (23) (2017) 28612–28618.

[6] P. Dong, R. Shafiiha, S. Liao, H. Liang, N. Feng, D. Feng, G. Li, X. Zheng, A. Krishnamoorthy, M. Asghari, Wavelength-tunable silicon microring modulator, Opt. Express 18 (11) (2010) 10941–10946.

[7] M. Kues, C. Reimer, B. Wetzel, P. Roztocki, B.E. Little, S.T. Chu, T. Hansson, E.A. Viktorov, D.J. Moss, R. Morandotti, Passively mode-locked laser with an ultra-narrow spectral width, Nature Photon. 11 (3) (2017) 159–162.

[8] S. Cho, R. Soref, Interferometric microring-resonant 2×2 optical switches, Opt. Express 16 (17) (2008) 13304–13314.

[9] L. Fan, J. Wang, L. Varghese, H. Shen, B. Niu, Y. Xuan, A. Weiner, M. Qi, An all-silicon passive optical diode, Science 335 (6067) (2012) 447–450.

[10] M. Bahadori, M. Nikdast, S. Rumley, L. Dai, N. Janosik, T. Vaerenbergh, A. Gazman, Q. Cheng, R. Polster, K. Bergman, Design space exploration of microring resonators in silicon photonic interconnects: impact of the ring curvature, Opt. Express 36 (13) (2018) 2767–2782.

[11] J. Heebner, R. Grover, T. Ibrahim, Optical Microresonators: Theory, Fabrication, and Applications, Springer, 2008.

[12] F. Xia, L. Sekaric, Y. Vlasov, Ultracompact optical buffers on a silicon chip, Nature Photon. 1 (1) (2007) 65–71.

[13] P. Dong, N.-N. Feng, D. Feng, W. Qian, H. Liang, D.C. Lee, B.J. Luff, T. Banwell, A. Agarwal, P. Toliver, R. Menendez, T.K. Woodward, M. Asghari, GHZ-bandwidth optical filters based on high-order silicon ring resonators, Opt. Express 18 (23) (2010) 23784–23789.

[14] L. Zhuang, C. Roeloffzen, A. Meijerink, M. Burla, D. Marpaung, A. Leinse, M. Hoekman, R. Heideman, W. Etten, Novel ring resonator-based integrated photonic beamformer for broadband phased array receive antennas-part II: Experimental prototype, J. Lightw. Technol. 28 (1) (2010) 19–31.

[15] A. Li, T.V. Vaerenbergh, P.D. Heyn, P. Bienstman, W. Bogaerts, Backscattering in silicon microring resonators: a quantitative analysis, Laser Photon. Rev. 10 (3) (2016) 420–431.

[16] A. Li, W. Bogaerts, An actively controlled silicon ring resonator with a fully tunable Fano resonance, APL Photon. 2 (9) (2017) 096101.

[17] M. Huang, S. Li, M. Xue, L. Zhao, S. Pan, Flat-top optical resonance in a single-ring resonator based on manipulation of fast- and slow-light effects, Opt. Express 26 (18) (2018) 23215–23220.

[18] S. Pan, M. Xue, Ultrahigh-resolution optical vector analysis based on optical single-sideband modulation, J. Lightw. Technol. 35 (4) (2017) 836–845.

[19] M. Xue, S. Liu, S. Pan, High-resolution optical vector analysis based on symmetric double-sideband modulation, IEEE Photon. Technol. Lett. 30 (5) (2018) 491–494.